JVST A
Journal of Vacuum Science & Technology A

ARTICLE

avs.scitation.org/journal/jva

Atmospheric pressure plasma functionalization of polystyrene

Cite as: J. Vac. Sci. Technol. A **40**, 043001 (2022); doi: 10.1116/6.0001850
Submitted: 4 March 2022 · Accepted: 12 April 2022 ·
Published Online: 10 May 2022

Jordyn Polito,[1,a] Mark Denning,[2,b] Richard Stewart,[3,c] David Frost,[3,d] and Mark J. Kushner[4,e]

AFFILIATIONS

[1]Department of Chemical Engineering, University of Michigan, 1221 Beal Ave., Ann Arbor, Michigan 48109-2102
[2]Agilent Technologies Inc., 5301 Stevens Creek Blvd., Santa Clara, California 95051-7201
[3]Agilent Technologies Inc., 300 Griffith Rd., Chicopee, Massachusetts 01022-2126
[4]Department of Electrical Engineering and Computer Science, University of Michigan, 1301 Beal Ave., Ann Arbor, Michigan 48109-2122

[a]**Electronic mail:** jopolito@umich.edu
[b]**Electronic mail:** mark.denning@agilent.com
[c]**Electronic mail:** richard.stewart@agilent.com
[d]**Electronic mail:** david.frost@agilent.com
[e]**Author to whom correspondence should be addressed:** mjkush@umich.edu

ABSTRACT

Atmospheric pressure plasma jets (APPJs) are used to improve the adhesive and hydrophilic properties of commodity hydrocarbon polymers such as polypropylene, polyethylene, and polystyrene (PS). These improvements largely result from adding oxygen functional groups to the surface. PS functionalization is of interest to produce high value biocompatible well-plates and dishes, which require precise control over surface properties. In this paper, we discuss results from a computational investigation of APPJ functionalization of PS surfaces using $He/O_2/H_2O$ gas mixtures. A newly developed surface reaction mechanism for functionalization of PS upon exposure to these plasmas is discussed. A global plasma model operated in plug-flow mode was used to predict plasma-produced species fluxes onto the PS surface. A surface site balance model was used to predict oxygen-functionalization of the PS following exposure to the plasma and ambient air. We found that O-occupancy on the surface strongly correlates with the O-atom flux to the PS, with alcohol groups and cross-linked products making the largest contributors to total oxygen fraction. Free radical sites, such as alkoxy and peroxy, are quickly consumed in the post-plasma exposure to air through passivation and cross-linking. O-atom fluences approaching 10^{17} cm^{-2} saturate the O-occupancy on the PS surface, creating functionality that is not particularly sensitive to moderate changes in operating conditions.

I. INTRODUCTION

Low temperature plasmas are often used to improve the wettability and adhesive properties of saturated hydrocarbon polymers such as polyethylene (PET), polypropylene (PP), and polystyrene (PS).[1–5] A common method for improving the adhesion and wettability of a polymer utilizes oxygen containing plasmas to attach oxygen and oxygen containing functional groups to the polymer surface. The added oxygen increases surface energy leading to more hydrophilic surfaces. Sources for plasma-surface modification range from low pressure glow discharges[6–9] to atmospheric pressure dielectric barrier discharges (DBDs) or corona.[10] Low pressure systems are often used where UV light or high energy ions are important to the functionalization process while there is added cost for the associated vacuum processing. Atmospheric pressure DBDs, often sustained in ambient air and having a lower cost, are typically used for high volume functionalization of commodity polymers.[11]

Atmospheric pressure plasma jets (APPJs) have been recently adopted for surface functionalization of polymers.[12,13] APPJs typically consist of a rare gas (or a rare gas mixture containing up to a few percent of an additive) flowing through a tubular plasma source into ambient air and onto the polymer surface. The plasma is produced in the tube with a pulsed or radio frequency voltage to generate a plume of plasma extending into the ambient air.[14] Other configurations confine the plasma to a flow channel using parallel radio frequency (RF) powered electrodes that largely confine the

plasma to the device. Here, the activated species in the plume consist dominantly of neutral radicals. Similar to DBDs, these systems offer advantages over low pressure discharges in that they do not require expensive vacuum equipment, allowing for larger surfaces of polymer to be processed in either batch or continuous modes. The disadvantage of APPJs relative to DBDs sustained in air is that the APPJs typically require high flow rates of rare gases with their associated costs. APPJs using rare gases should, therefore, usually be reserved for high value processes. APPJs tend to produce higher fluxes of reactive oxygen species (ROS) compared to DBDs sustained in air, which is advantageous for surface functionalization applications where improved hydrophilic and adhesive properties by the addition of oxygen are desired.

Improving the wettability of polymers by the addition of oxygen groups is of particular interest to the biological science and biomedical engineering communities. These communities often require polymeric materials to be in direct contact with living organisms. The oxygen functionality is used either directly (being more hydrophilic) or as a base for attaching more biologically active groups, such as amines. Surface characteristics that can influence cellular interactions with the polymer, such as surface energy and wettability, are important when choosing the polymer appropriate for the desired application.[15,16] PS is often used for cell culturing substrates (e.g., well-plates, Petri dishes) due to its low toxicity and long shelf life of the plasma-produced functionality after treatment.[17,18]

The fixing of oxygen to a polymer surface improves wettability and adhesion by increasing the surface energy, thereby increasing hydrophilicity. APPJs consisting of Ar/O_2, Ar/H_2O, He/O_2, and N_2/O_2 gas mixtures, among others, have been used for polymer modification with varying success of increasing hydrophilicity.[19–21] Water contact angle measurements that relate the angle of water spreading on the polymer surface with surface energy through Young's equation are the most common methods for determining the degree of functionalization that has occurred on a polymer surface after plasma treatment.[2,22] Decreases in the contact angle correlate with an increase in wettability and are thought to be due to the addition of alcohol, carbonyl, ketone, and aldehyde functional groups. These groups have been experimentally characterized on the surface of plasma-treated PS by x-ray photoelectron spectroscopy (XPS) measurements.[23–27] While water contact angle measurements and XPS measurements independently confirm that plasma-treated PS has some degree of functionalization, there is no formulaic relationship between the measured contact angle and the occupancy of each functional group on the surface after plasma treatment. This lack of direct correlation makes optimization of the functionalization process more difficult. Computational modeling, when paired with experimental measurements, can be a useful tool in determining the chemistry of a plasma-treated polymer surface.

Several models have addressed plasma functionalization of polymers, but they are largely limited to PP due to its wide industrial use and relatively simple monomer unit. Wang *et al* related contact angle and XPS measurements to functional groups on a PP surface after treatment by an atmospheric pressure air DBD.[28] Their regressive model was able to predict changes in contact angle as a function of percentage of O atoms on the PP surface for their DBD conditions. A robust method for predicting surface functionalization is to couple a plasma chemistry model that predicts fluxes to surfaces with a surface site balance model that predicts the evolution of surface properties. The functionalization of PP has been modeled with this technique using fluid and global model techniques.[29–31] These models predicted the fractional occupation of functional groups on the PP surface as functions of plasma operating conditions on rough and smooth surfaces.

These models have the potential to be extended to investigate the plasma functionalization of other commodity polymers, However, as the polymer monomer units become more complex, reaction mechanisms for the functionalization of the polymers become increasingly unclear. For example, the presence of aromatic rings in the monomer units of polymers such as PS and polycarbonate raises issues of steric hindrance and reactivity of the aromatic ring, compared to other sites on the polymer backbone. Investigations have addressed how aromatic compounds such as benzene or toluene interact in plasmas.[32–34] Investigations have also been performed to predict the final configurations of oxygen functional groups on a modified PS surface using density functional theory (DFT) and ab initio molecular dynamics (MD) techniques.[35] These simulations suggest that initiation of oxygenation of PS results from insertion of O atoms into C–H bonds to form C–OH. As the surface becomes more oxygenated, alcohol, ester, and carbonyl groups are formed, including ring breaking. These processes are temperature dependent, particularly, with respect to oxygen penetration below the nominal surface.

In this paper, a reaction mechanism for the functionalization of PS by a He/O_2 APPJ is proposed. Results are discussed from a computational investigation of coupled global plasma chemistry and surface-site-balance models using this reaction mechanism for the surface functionalization of PS after APPJ treatment and post-treatment exposure to ambient air. The global model is used in a plug-flow mode to provide the plasma-produced reactive species that exit the reactor, mix with ambient air and impinge upon a flat PS surface. A surface site balance model is used to track changes in the fractional occupancy of surface groups due to gas-surface and surface-surface reactions. The plasma-treated surface is then exposed to ambient humid air to simulate short-term aging of the functionalized surface. The functionalization of the PS in terms of fractional occupancy of oxygen on the surface as a function of power, gas composition, and humidity is discussed. We found that parameters affecting O production, such as power and inlet gas composition, offer the largest degree of control for optimizing the O-occupancy on the PS surface. We predict that alcohol and cross-linked groups make up the largest contribution of O-containing functional groups on the PS surface after APPJ treatment and exposure to ambient air.

The models used in this investigation are described in Sec. II. The surface reaction mechanism is discussed in Sec. III. Base case plasma properties and parametric studies examining the change in oxygen content on the PS surface are discussed in Secs. IV and V. Concluding remarks are in Sec. VI.

II. DESCRIPTION OF THE MODEL

The model used in this work, *GlobalKin*, is a zero-dimensional plasma chemistry simulator that accounts for the electron impact, ion and neutral particle reactions, gas flow, plasma-surface

interactions, and surface kinetics. *GlobalKin* is discussed in detail elsewhere[36,37] and so will be described only briefly here. The densities of gas-phase species are derived using continuity equations that account for sources and losses due to electron impact, ion molecule and neutral reactions, flow, and diffusion to the wall. Assuming quasineutrality, the flux of positive ions to the wall occurs with an ambipolar enhanced rate equal to the sum of the fluxes of negative ions and electrons. From a practical perspective, the flux of negative ions to the walls is negligible in the power deposition regions due to their being trapped in the positive plasma potential.

The electron energy equation is solved for the average electron temperature. Electron energy distribution functions are obtained from solutions of the stationary Boltzmann's equation over a range of E/N (electric field/gas number density) values, which are stored in lookup tables with the independent variable being electron temperature. The table is then interpolated during the execution of the model to provide reaction rate coefficients and transport coefficients for the current electron temperature. The lookup table is periodically updated to reflect changes in gas mole fractions.

The reactor is a linear flow radio frequency (RF) excited plasma. Power (W/cm^3) is specified as a function of position in the flow direction with the integral over volume having the desired total power deposition. The specific power (W/cm^3) as a function of position is used as input to the electron energy equation. The gas temperature is determined by accounting for the elastic power transfer from electrons to atoms and molecules, Franck–Condon heating due to dissociative processes (e.g., electron impact dissociative excitation and dissociative recombination), charge exchange heating from hot ions accelerated in the ambipolar electric field, the change in enthalpy due to chemical reactions, and heat conduction to the walls.

Gas flow is represented using a plug-flow approximation, which follows a slug of gas transporting through a channel having a cross sectional area $A = WD$, where W is the width of the electrode and D is the dimension of the gap between the electrodes. The gas plug moves down the length of the reactor with an initial speed determined by the input flow rate (SCCM), gas density, and cross sectional area A. With subsonic flow, the system is isobaric (constant pressure). The flow speed is then adjusted as dissociation increases the total inventory of atoms and molecules, and the gas is heated (or cooled) to keep the pressure constant.

Flow between the electrodes occurs with the initially specified input mole fractions until exiting the plasma source. At this time, there is mixing with the ambient air. To approximate this mixing, a specified mole fraction of humid air is introduced into the flow. This mole fraction was obtained by performing 2-dimensional computational fluid dynamics simulations of the reactor geometry for a He jet flowing into humid air. The average air content in the He jet was then used as the mole fraction of the ambient air introduced into the plug flow.

The polymer surface being treated is a specified distance from the outlet of the plasma source. In principle, the flow from the plasma source arrives perpendicular to the surface and produces a stagnation layer. Reactants then diffuse through the stagnation layer to reach the surface. The diffusion length from the bulk flow through the stagnation layer to the surface is approximated as the thickness of the flow boundary layer.

The fluxes of ions and neutrals to the surface being treated are used as an input to the surface kinetics module (SKM) for predicting the composition of the surface. The SKM consists of a set of rate equations for the surface density of sites (or fractional surface coverage) of surface resident species. The surface site balance accounts for the rates of adsorption, abstraction, and desorption resulting from incident gas-phase fluxes and reactions between surface species. The site balance equation is

$$\frac{\partial \theta_j}{\partial t} = -\theta_j \left(\sum_i \phi_i p_{ij} + \sum_m \theta_m p'_{jm} \right) + \sum_{i,m} \theta_m \phi_i p_{imj} + \sum_{l,m} \theta_l \theta_m p'_{lmj}, \tag{1}$$

where θ_j is the surface site coverage of species or group j, ϕ_i is the incident flux of gas-phase species i, p_{ij} is the total reaction probability of gas-phase species i with surface species j, p_{imj} is the probability of reaction between gas-phase species i and surface species m that produces surface species j, p'_{jm} is the total probability of reaction between surface sites j and m, and p'_{lmj} is the total probability of reaction between surface species l and m to produce surface species j.

The aging of plasma-treated polymers is a well-known phenomenon. Aging is an evolution of the surface properties after the plasma treatment that may occur over a few minutes to many days or weeks.[38,39] For example, the air plasma treatment of polypropylene increases the surface oxygen content and reduces the water contact angle as an indication of making the surface more hydrophilic.[40] Following plasma treatment, the water contact angle will increase from its minimum post-treatment value. The cause of aging is poorly known and may be attributed to slow reactions between surface species that reduce the exposure of oxygen groups on the surface, reactions with the ambient air, and/or the release of treatment-induced stress on the surface which rotates oxygen groups away from the surface.[41,42]

To simulate aging with the SKM, after the specified plasma treatment time, the plasma-produced gas-phase fluxes to the surface are replaced by diffusive fluxes of ambient humid air. The SKM is executed for additional time until the surface composition achieves a near steady state. The same surface reaction mechanism is used by the SKM during the plasma treatment and during post-treatment by the ambient humid air. The surface reaction mechanism is discussed in Sec. III.

III. SURFACE REACTION MECHANISM

PS is a saturated hydrocarbon polymer whose monomer unit contains an aromatic benzene ring (denoted with subscript b in the following), two H atoms at secondary sites (denoted with subscript 2), and an H atom at a tertiary site (denoted with subscript 3) (see Fig. 1). Commercially available PS is atactic, meaning its monomer units are configured randomly such that there is an equal likelihood for any of the four groups (benzene ring or H atoms) to be oriented toward the surface of the material. However, the benzene ring is physically larger than the neighboring sites, which may result in the benzene ring obscuring neighboring sites as a form of steric hindrance. The density of PS surface sites in the

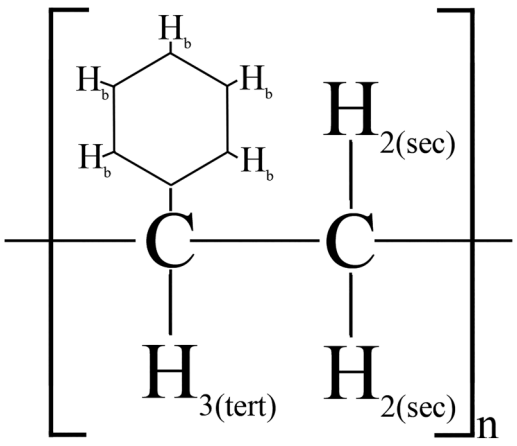

FIG. 1. Polystyrene monomer unit.

model is initialized as 10^{15} cm^{-2}, in agreement with the available molecular dynamics data and reported values for other polymeric materials.[30,43] The density of benzene sites, N_b, is initially 0.5×10^{15} cm^{-2}. The initial surface densities for the secondary and tertiary H atoms are $N_2 = N_3 = 0.25 \times 10^{15}$ cm^{-2}.

The model includes 71 gas-phase species and 33 surface species. The gas-phase species included in the model are listed in Table I. The gas-phase reaction mechanism for a He/O_2 atmospheric plasma has been discussed in detail in prior studies.[29,30] In short, atomic oxygen is produced primarily through the electron impact dissociation of O_2 (neutral and dissociative attachment) and by dissociative Penning reactions with excited states of He. O atoms are consumed dominantly through three-body collisions with O_2 to form ozone, O_3. O_2 is also electronically excited by collisions with electrons to form $O_2(^1\Delta)$ and $O_2(^1\Sigma)$. If water vapor is present in the plasma, H_2O is dissociated by electron impact to form OH and H and by Penning reactions with excited states of He. Reactions of O_3 with H lead to the formation of OH, while reactions of O_3 with OH lead to the formation of HO_2. Positive ions, O^+, O_2^+, and H_2O^+ are produced by electron impact ionization of O, O_2, and H_2O; by charge exchange from He^+ and He_2^+; and by Penning reactions with excited states of helium. Formation of negative ions is dominated by three-body electron attachment to O_2 to form O_2^- at atmospheric pressure. Plasma-produced ion densities in the system are 2–3 orders of magnitude lower than the neutral plasma-produced reactive oxygen species (ROS). The gas-phase species in the model that react with the PS to promote oxidation are O_2* (sum of electronically excited states of O_2), O_3, O, H, OH, and HO_2.

TABLE I. Gas-phase species included in plasma chemistry model.

Hydrogen species[a,b]
H, H*, H^+, H^-, H_2, $H_2(r)$, $H_2(v)$, H_2^+, H_2*, H_3^+
Oxygen species[a,b]
O_2, $O_2(r)$, O_2 (v), O_2*, $O_2(^1S)$, O_2^+, O_2^-, O, O*, O^+, O^-, O_3, O_3*, O_3^-, O_4^+
Nitrogen species[a,b]
N_2, $N_2(r)$, $N_2(v)$, N_2*, N_2^+, N_3^+, N_4^+, N, N*, N^+
Helium species[a]
He, He^+, He, $He_2(^1S)$, $He_2(^3P)$, $He_2(^1P)$, $He(^3P)$, $He(^3S)$, He_2*, He_2^+
Heterogenous species[a,b]
OH, OH*, OH^-, H_2O, $H_2O(v)$, H_2O^+, HO_2, H_2O_2, H_3O^+, NO, NO_2, NO_2^+, NO_2^-, NO_3, NO_3^-, N_2O, $N_2O(v)$, NH, HNO, HNO_2, HNO_3, HNO_4, $H_4O_2^+$, $H_2O_3^+$, $H_5O_2^+$, HeH^+

[a]* denotes an excited state atom or molecule.
[b](r) and (v) denote rotationally and vibrationally excited molecules, respectively.

As PS and PP share the same monomer units except for one group, the surface reaction mechanism closely follows that for the functionalization of PP previously discussed in Ref. 29. Changes were made to the mechanism to account for reactions with the benzene ring in PS rather than with the methyl group in the PP monomer unit. Some values of reaction probabilities have been adjusted from those discussed in Refs. 29 and 30 as discussed below. The full gas-surface reaction mechanism is listed in Table II. In several cases, reaction probabilities between the gas-phase and surface resident species were approximated by analogy to gas-phase reactions. For example, H abstraction from benzene in the gas phase has a rate coefficient of k. The rate coefficient was normalized by the gas kinetic rate coefficient k_0, representing the fastest possible rate of reaction. The probability of reaction is then $p = k/k_0$. This probability was assigned to the analogous surface reaction of a gas-phase species abstracting an H atom from the aromatic ring in the PS backbone. These probabilities might be further derated by steric hindrances. The analogous gas-phase reactions that were used to estimate gas-surface reaction probabilities are in Appendix, Table III.

Oxidation of the PS surface is a three-step mechanism that begins with the abstraction of hydrogen from the polymer chain to form an alkyl radical site or from the benzene ring to form a phenyl radical site. Reactivity of the surface sites scale with the activation energy required to remove the H atom at that site such that the probabilities of reaction scale as $p(H_3) > p(H_2) > p(H_b)$ (see Fig. 1). After the H abstraction, gas-phase species (O, O_2, O_3, O*, OH) react with the surface radical sites to form oxygen containing radical sites or terminate the site by the formation of alcohol, aldehyde, or hydroperoxyl functional groups.

Etching of the PS surface was not included in this mechanism. Low molecular weight materials on the polymer surface after plasma treatment are indicative of polymer etching.[55,56] However, even under low pressure conditions where ion fluxes to the surface were high, significant amounts of low molecular weight materials were not found on the PS surface after plasma exposure for less than 1 hour.[55,57] Recently, the etching probabilities for APPJ-produced O, H, and OH radical species incident onto a PS surface have been reported.[58,59] The etching rate due to OH was reported to be the highest with a probability on the order of 10^{-2} for an Ar/H_2O plasma with an OH radical density of 10^{14} cm^{-3}, suggesting that the removal of one C atom occurs for every 100 OH radicals.[58] PS etching was highly sensitive to the oxygen content in

TABLE II. Surface reaction mechanism.

Surface species	
R_n–H (b = benzene ring 2 = secondary 3 = tertiary)	PS backbone
R_n–•	Alkyl
R_n—O•	Alkoxy
R_n—OO•	Peroxy
R_n—OH	Alcohol
R_n—OOH	Hydroperoxide
HR_n═O	Carbonyl
R_n—OO—R_n	Cross-link product
R_n—O—R_n	Cross-link product

	Reaction	Probability or reaction rate coefficient[a]	Comments
	Gas-phase surface reactions		
1	$O + R_3–H \rightarrow OH + R_3–•$	5×10^{-3}	c
2	$O + R_2–H \rightarrow OH + R_2–•$	5×10^{-4}	c
3	$O + R_b–H \rightarrow OH + R_b–•$	3.31×10^{-4}	b
4	$OH + R_3–H \rightarrow H_2O + R_3–•$	0.5	c
5	$OH + R_2–H \rightarrow H_2O + R_2–•$	0.5	c
6	$OH + R_b–H \rightarrow H_2O + R_b–•$	6.61×10^{-3}	b
7	$HO_2 + R_3–H \rightarrow H_2O_2 + R_3–•$	5×10^{-5}	c
8	$HO_2 + R_2–H \rightarrow H_2O_2 + R_2–•$	5×10^{-5}	c
9	$O + R_3–• \rightarrow R_3–O•$	0.5	c
10	$O + R_2–• \rightarrow R_2–O•$	0.5	c
11	$O + R_b–• \rightarrow R_b–O•$	1.0	b
12	$O_2 + R_3–• \rightarrow R_3–OO•$	2×10^{-3}	c
13	$O_2 + R_2–• \rightarrow R_3–OO•$	4.4×10^{-4}	c
14	$O_2 + R_b–• \rightarrow R_b–OO•$	5.83×10^{-2}	b
15	$O_3 + R_3–• \rightarrow R_3–OO• + O_2$	1.0	c
16	$O_3 + R_2–• \rightarrow R_2–OO• + O_2$	0.5	c
17	$O_3 + R_b–• \rightarrow R_b–OO• + O_2$	1.0	b
18	$O + R_b–O• \rightarrow R_b–OO•$	0.626	b
19	$NO + R_3–O• \rightarrow R_3–• + NO_2$	0.1	c
20	$NO + R_2–O• \rightarrow R_2–• + NO_2$	0.1	c
21	$NO + R_b–O• \rightarrow R_b–• + NO_2$	3.6×10^{-2}	b
22	$O + R_3–OH \rightarrow R_3–O• + OH$	7.5×10^{-4}	c
23	$OH + R_3–OH \rightarrow R_3–O• + H_2O$	8.2×10^{-3}	c
24	$OH + R_b–OH \rightarrow R_b–O• + H_2O$	2.18×10^{-2}	b
	Surface-surface reactions		
25	$R_3–OO• + R_3–H \rightarrow R_3–OOH + R_3–•$	5.5×10^{-16}	c
26	$R_2–OO• + R_2–H \rightarrow R_2–OOH + R_2–•$	5.5×10^{-16}	c
27	$R_b–OO• + R_3–H \rightarrow R_b–OOH + R_3–•$	5.5×10^{-17}	e
28	$R_b–OO• + R_2–H \rightarrow R_b–OOH + R_2–•$	1.1×10^{-18}	e
29	$R_3–O• + R_3–H \rightarrow R_3–OH + R_3–•$	2×10^{-14}	c
30	$R_3–O• + R_2–H \rightarrow R_3–OH + R_2–•$	4×10^{-14}	c
31	$R_3–O• + R_b–H \rightarrow R_3–OH + R_b –•$	2×10^{-16}	c, d
32	$R_2–O• + R_3–H \rightarrow R_2–OH + R_3–•$	2×10^{-14}	c
33	$R_2–O• + R_2–H \rightarrow R_2–OH + R_2–•$	4×10^{-14}	c
34	$R_2–O• + R_b–H \rightarrow R_2–OH + R_b–•$	4×10^{-16}	c, d
35	$R_b–O• + R_3–H \rightarrow R_b–OH + R_3–•$	7.5×10^{-14}	c, d
36	$R_b–O• + R_2–H \rightarrow R_b–OH + R_2–•$	7.5×10^{-14}	c, d
37	$R_2–O• + R_3–OOH \rightarrow R_2–OH + R_3–OO•$	1×10^{-20}	c
38	$R_2–O• + R_2–OOH \rightarrow R_2–OH + R_3–\ OO•$	1×10^{-20}	c
39	$R_b–• + R_3–H \rightarrow R_b–H + R_3–•$	7×10^{-14}	d
40	$R_b–• + R_2–H \rightarrow R_b–H + R_2–•$	7×10^{-14}	d
41	$R_b–• + R_2–OH \rightarrow R_b–H + R_2–O•$	1×10^{-14}	b

TABLE II. (*Continued.*)

	Reaction	Probability or reaction rate coefficient[a]	Comments
42	$R_b–• + R_3–OH \rightarrow R_b–H + R_3–O•$	1×10^{-14}	b
	Cross-linking reactions[g]		
43	$R_b–O• + R_b–O• \rightarrow R_b–OO–R_b$	3×10^{-11}	f
44	$R_n–OO• + R_m–OO• \rightarrow R_n–OH + HR_m{=}O + O_2$	2.4×10^{-14}	f
45	$R_n–OO• + R_n–OO• \rightarrow R_n–OO–R_n + O_2$	4×10^{-14}	f
46	$R_n–OO• + R_m–OO• \rightarrow R_n–OO–R_m + O_2$	1×10^{-14}	f
	Gas-phase termination reactions		
47	$H + R_3–• \rightarrow R_3–H$	0.2	c
48	$H + R_2–• \rightarrow R_2–H$	0.2	c
49	$H + R_b–• \rightarrow R_b–H$	1.0	b
50	$HO_2 + R_b–• \rightarrow R_b–OOH$	1.0	b
51	$OH + R_3–OO• \rightarrow R_3–OH + O_2$	5×10^{-5}	c
52	$OH + R_2–OO• \rightarrow R_2–OH + O_2$	5×10^{-5}	c
53	$OH + R_b–O• \rightarrow R_b–OOH$	9.29×10^{-12}	b
54	$HO_2 + R_3–OO• \rightarrow R_3–OOH + O_2$	5×10^{-5}	c
55	$HO_2 + R_2–OO• \rightarrow R_2–OOH + O_2$	5×10^{-5}	c
54	$HO_2 + R_3–O• \rightarrow R_3–OH + O_2$	0.50	b
55	$HO_2 + R_2–O• \rightarrow R_2–OH + O_2$	0.50	b
56	$OH + R_3–• \rightarrow R_3–OH$	1×10^{-5}	c
57	$OH + R_2–• \rightarrow R_2–OH$	1×10^{-5}	c

[a]Reaction rates for gas-surface reactions are written as probabilities. Reaction rates for surface-surface reactions have units of cm^2/s.
[b]Reaction rate is approximated from an analogous gas-phase reaction with a long chain alkane from the NIST database.[44] Analogs and their references are listed in the Appendix.
[c]Reaction rates are adjusted from those given in Bhoj and Kushner (Ref. 29).
[d]Reaction rates estimated from Park *et al.* (Ref. 45).
[e]Reaction rates estimated from Rabek *et al.* (Ref. 34).
[f]Reaction rates for cross-linking reactions are estimated from Atkinson *et al.* (Ref. 46).
[g]m and n represent any combination of surface group.

the environment between the reactor outlet and the PS surface.[60] In cases where the plasma jet was not shielded and the local oxygen concentration was that of ambient air, etching was much less significant than in cases where the plasma jet was shielded. This result was likely a consequence of the consumption of O and OH. The system under study is not shielded and has an OH flux to the surface on the order of $10^{14}\,cm^{-2}\,s^{-1}$, 3–4 orders of magnitude smaller than the flux of OH reported in Ref. 58. We expect etching to be negligible for our system.

Chain scission or the breakings of bonds in the middle of a polymer chain has also been neglected in this mechanism. Chain scission has been shown to occur in studies of the plasma treatment of polymers such as PP, PE, and PMMA; however, chain scission has not been observed in the treatment of PS having no prior oxidation.[56,61,62] Experiments of PS treated by a low pressure Ar/O_2 plasma determined that PS is prone to chain scissions after oxidation or treatment times much greater than those addressed here.[26] The lack of chain scissions in plasma-treated PS is thought to be due to the presence of the benzene ring, which stabilizes the PS backbone by trapping and redistributing energy.[3] There still remains the possibility that chain scissions could occur at the end of the polymer chain where the trapping and redistribution of energy by the benzene ring may not be as pronounced. We have assumed that chain ends do not make up a significant portion of our sample and have neglected chain scission.

Cross-linking occurs when a surface radical site on one polymer chain reacts with a radical site on another polymer chain as a form of lowering surface energy. Cross-linking has been shown to occur on the surface of plasma-treated PP and PS and can contribute to increased surface adhesion and wettability.[62–64] A cross-linking mechanism has been included as a means of terminating radical sites and so stabilizing the surface functionalization against further aging. In the proposed mechanism, cross-linking occurs between two peroxy radical sites or between phenoxy sites. While cross-linking may occur during plasma treatment, we expect the majority of cross-linking to occur in the post-treatment exposure to ambient air. During this time, the fluxes of reactive species to the surface, and, therefore, the termination of radical sites by those species is essentially zero, while the duration of the post-treatment is longer than that of the plasma treatment.

IV. BASE CASE PLASMA PROPERTIES

The plasma device investigated here is based on commercial plasma sources used to functionalize polymers for biotechnology applications. A schematic of the reactor geometry used in the model is shown in Fig. 2. For the base case, 45 slm (standard liters/min) SLM of a $He/O_2 = 98/2$ gas mixture with a water vapor impurity of 10 ppm flows into the top of a plasma head at atmospheric pressure. The gas mixture flows between a set of electrodes having a length of 10 cm, a width of 10 cm, and a separation of 0.2 cm. The power deposition is 210 W which we assume produces a uniform discharge over the electrode area. The gas flow exits the plasma head through a slot located 10 cm from the inlet and mixes with humid air ($N_2/O_2/H_2O = 77.5/20/2.5$) in a 2 mm gap between the plasma head and the PS surface. The rate of diffusion of air into the plasma plume was approximated as 1% of the inlet flow rate based on 2-dimensional computational fluid dynamics modeling.

Densities of gas-phase species for the base case conditions are shown in Fig. 3. The base case conditions yield a plasma with an electron density, n_e, on the order of 10^{10} cm^{-3} and an average electron temperature, T_e, of 2.5 eV, which is consistent with reported values for rf-driven APPJs.[65–67] While not shown in Fig. 3(a), the gas temperature increases down the length of the reactor from 300 K to about 312 K before decreasing to 300 K in the air gap. (With the narrow electrode gap, the heat conduction to the walls of the discharge, held at 300 K, is efficient.) O_2*, O_3, and O are the primary ROS exiting the reactor to mix with the air. O_2* (5×10^{16} cm^{-3}) and O (3×10^{15} cm^{-3}) are formed with high densities downstream as electronic excitation and electron impact dissociation of O_2 are the main sources of energy dissipation in this system. O_3 (1.6×10^{16} cm^{-3}) is formed dominantly through three-body collisions between He, O, and O_2. O_3 is formed at the same rate as O near the top of the reactor before reaching a steady state value that is constrained by the low mole fraction of O_2. Significant densities of H (2×10^{13} cm^{-3}) and OH (2×10^{13} cm^{-3}) are produced by electron impact dissociation of H_2O and excitation transfer from He*, as a result of the water impurity. HO_2 (2×10^{13} cm^{-3}) is produced as a product of reactions of OH with O_3 and H_2 with O_2. The O density decreases in the air gap after exiting the reactor due to reactions with H_2O and H_2O dissociation products to form more energetically favorable molecular species OH, H_2, O_2, and H_2O.

The resulting functionalization of the PS surface by these ROS fluxes is shown in Fig. 4(a). The PS surface was exposed to the plasma plume for 12 s, which corresponds to a polymer web speed of 10 cm/min for this configuration. After plasma treatment, the PS surface is exposed to ambient air for 200 s.

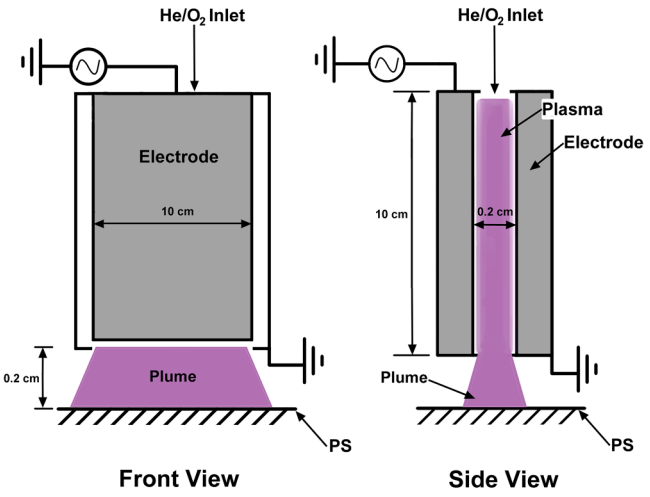

FIG. 2. Front and side views of plasma head geometry used in the model. A He/O_2 mixture at atmospheric pressure is flowed between parallel plate electrodes separated by 2 mm, with the plume flowing into the ambient air.

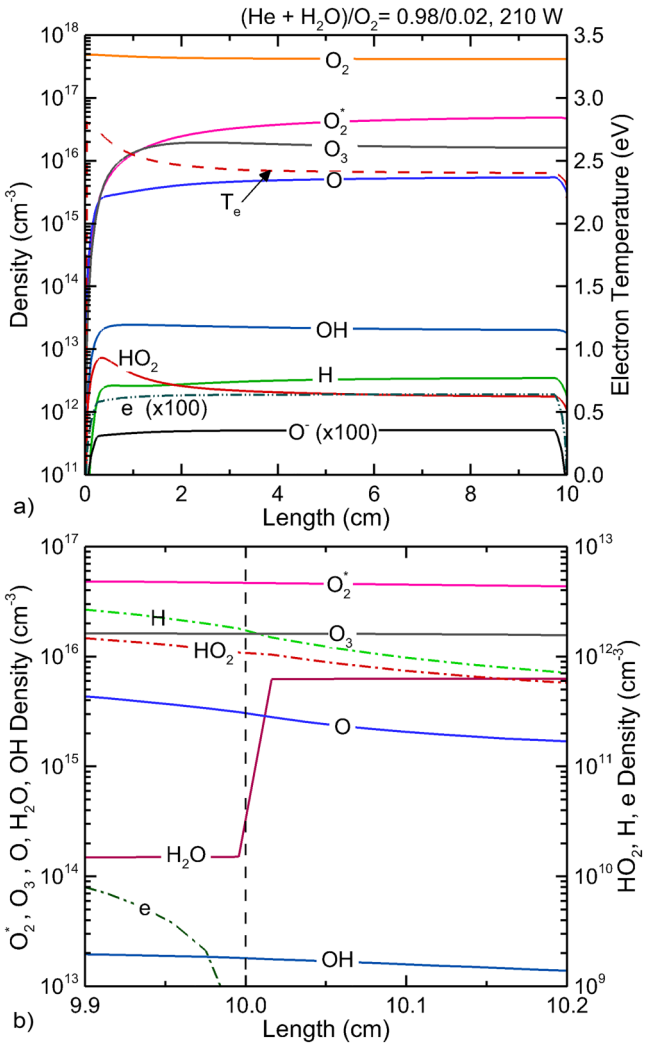

FIG. 3. Base case plasma properties (Pressure = 1 atm, $He/O_2/H_2O = 98/2/10$ ppm, Power = 210 W, Gap = 2 mm, Ambient air = $N_2/O_2/H_2O = 78/20/2$). (a) In the reactor and (b) in the gap between the plasma head and the PS surface.

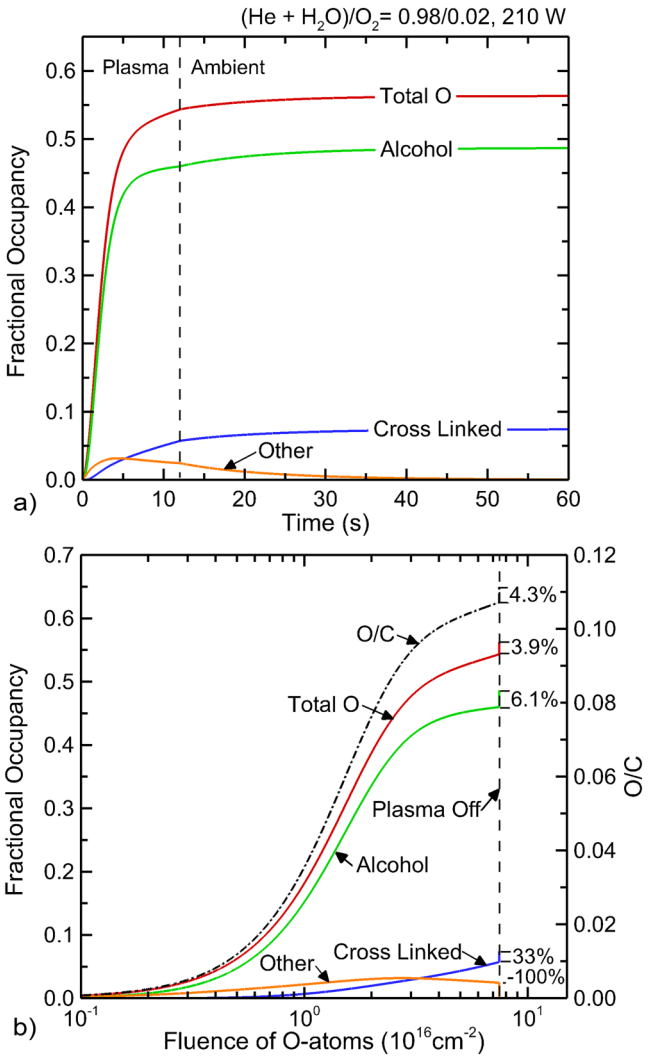

FIG. 4. Base case fractional occupancy of oxygen containing functional groups on the PS surface after plasma treatment and exposure to air. (a) Occupancy as a function of time for a plasma treatment time of 12 s and post-treatment time until 60 s. (b) Occupancy and the O/C ratio as a function of O-atom fluence. The tick marks and percentage after plasma turn-off denote the change in occupancy (or O/C ratio) during the post-plasma exposure to air.

(The entire post-treatment time is not shown in Fig. 4(a)). Exposure to ambient air serves mainly to terminate any free radical sites left on the PS surface after contact with the plasma, thereby stabilizing the surface. Changes in surface functionality due to exposure to ambient air occur only over the first 20 s after the plasma is turned off, at which time, a steady state oxygen fractional occupancy is achieved. Plasma-treated PS has been shown to maintain stability for up to 1 year.[18] We consider the steady state fractional occupancy of oxygen achieved after the first 20 s of post-treatment to be the final stable configuration of the modified polymer.

Total oxygen fractional occupancy on the PS surface shown in Fig. 4 increases linearly from 0% to 50% over the first half of the 12 s treatment time, with a more gradual increase to about 56% oxygen occupancy occurring in the latter half of the treatment time. The alcohol functional group makes the largest contribution to the total O-occupancy, accounting for a site occupancy of 48% when the final, stable configuration is achieved, or 86% of the total O-occupancy. The surface functionalization is dominantly initiated by H abstraction from the surface to form alkyl radical sites by the high flux of plasma-produced O to the surface, with secondary contributions by OH,

$$O + R_n{-}H \rightarrow OH + R_n{-}\bullet, \tag{2}$$

$$OH + R_n{-}H \rightarrow H_2O + R_n{-}\bullet, \tag{3}$$

where R_n is the PS monomer unit, with n = 2 for the secondary H site, 3 for the tertiary H site and b for the benzene ring.

There are three pathways for alcohol group formation after surface functionalization is initiated

$$OH + R_n{-}\bullet \rightarrow R_n{-}OH, \ n = 2, 3. \tag{4}$$

The first consists of the addition of OH formed as either plasma-produced ROS or as a product of H abstraction to an alkyl radical site [Eq. (4)]. In the second pathway, O and O_3 react with an alkyl site to form an alkoxy radical site. The alkoxy radical site can then abstract an H from a neighboring site,

$$O + R_n{-}\bullet \rightarrow R_n{-}O\bullet, \ n = 2, 3, b, \tag{5}$$

$$R_n{-}O\bullet + R_m{-}H \rightarrow R_n{-}OH + R_m{-}\bullet, \ n, m = 2, 3, b. \tag{6}$$

Finally, addition of O_2 to an alkyl site results in the formation of a peroxy group. The peroxy group undergoes a reaction with OH to form an alcohol group and O_2,

$$O_2 + R_n{-}\bullet \rightarrow R_n{-}OO\bullet, \ n = 2, 3, b, \tag{7}$$

$$OH + R_n{-}OO\bullet \rightarrow R_n{-}OH + O_2, \ n = 2, 3. \tag{8}$$

In the first half of the plasma treatment period, the next largest contributor to total oxygen coverage is the "other" group, comprised mostly of unterminated alkoxy radical sites. The next most abundant site is cross-linked products. Addition of O_2 to an alkyl site produces a peroxy group, which can participate in reactions with other peroxy groups to form cross-linked products,

$$R_n{-}OO\bullet + R_n{-}OO\bullet \rightarrow R_n{-}OO{-}R_n + O_2, \quad n = 2, 3, b. \tag{9}$$

In the latter half of the plasma treatment time, the "other" group begins to decrease as peroxy sites are terminated by these cross-linking reactions. Steady state total oxygen occupancy is approached as the formation of the alcohol group slows down in the latter half of the treatment time. When the plasma is turned off, total oxygen occupancy increases slightly to approach the steady state value of 56% as the remaining radical sites are

terminated (dominantly the alkoxy sites) in favor of a stable surface configuration. These base case results are consistent with experimental XPS measurements, which suggest that groups containing the C–O bond (alcohol or ether groups) make the largest contribution to the total oxygen fraction on the surface of plasma-treated PS.[26,56,68]

The oxygen occupancy on polymer films is often expressed as the O/C (oxygen-to-carbon) ratio, a value typically produced from XPS measurements. The O/C ratio was estimated for our results as a function of O-fluence to the PS surface and is shown in Fig. 4(b). Our estimates of the O/C ratio may be systematically lower than that given by XPS measurements. Plasma-treated PS samples typically have some degree of surface roughness after functionalization, which will increase the surface area available for measurements by the XPS. The treated sample in our simulations is conceptually perfectly flat. As the O-fluence approaches its maximum value (7×10^{16} cm^{-2}) near the end of the plasma treatment time, the O/C ratio on the surface approaches a steady state value of 11%. The trends and values in O/C estimated here are consistent with experimentally determined O/C from XPS measurements resulting from low pressure plasma-treated PS over similar ranges of O-fluence.[69] The saturation in O/C is a consequence of the low reactivity of the aromatic ring compared to the alkane components and the propensity for cross-linking.

The fluence of O atoms to the surface terminates when the plasma is turned off (or the surface is removed from the plasma plume). The surface continues to evolve by, for example, abstraction of H from surface sites by peroxy groups and the passivation of free radical sites by ambient O_2. The evolution of the surface composition post-plasma exposure is indicated by the double lines labeled with the percentage increase in Fig. 4(b). An increase in O-coverage of 3.9% occurs with post-plasma exposure, largely attributable to the formation of alcohol groups (6.1%) and cross-linked products (33%). This increase, in part, comes from a decrease in the coverage of alkoxy and peroxy groups of essentially 100%.

Experimental measurements show the C–O group as being the most abundant on PS surfaces when treated in atomic gas plasmas containing small amounts of O_2.[26,41,64] XPS measurements fail to differentiate whether the C–O bond belongs to an alcohol or an ether group. While reactions for ether group formation were included in the mechanism, the rates for alcohol formation are higher and dominate under our conditions.

V. SCALING OF O-OCCUPANCY ON PS

In this section, the dependence of O-occupancy of the PS surface will be discussed while varying the distance between the plasma source and the surface, O_2 mole fraction in the inlet flow, and humidity in the ambient.

A. Plasma source to PS surface distance

One of the process variables in PS functionalization is the distance between the plasma head and the PS surface. Since this is a remote plasma source, the plasma itself will not be altered and so the flux of reactive species leaving the plasma source does not directly depend on the source-surface distance. However, during the additional flow time to reach the surface, reactions occur in the plume, including reactions with the ambient air diffusing into the plume. The gap was varied between 1 and 20 mm to investigate how these changes in chemistry due to air diffusion into the plume affect the surface functionality.

The densities of gas-phase species in the gap between the plasma source and PS surface, for gap distances of 1, 5, 10, and 20 mm are shown in Figs. 5(a)–5(d). The fractional occupancy of oxygen containing groups on the PS surface after 12 s of the plasma treatment and 200 s of post-treatment air exposure are shown in Fig. 6. As the gap increases from 1 to 20 mm, the density of O reaching the PS surface decreases from 1×10^{15} to 8×10^{14} cm^{-3}, while the O_3 density decreases from 2×10^{16} to 1×10^{16} cm^{-3}. O atoms are consumed by reactions with O_2 to produce O_3 and with water vapor to form OH. Total O-occupancy decreases with increasing gap distance from 56% at 2 mm to about 45% at 20 mm. Alcohol is the dominant functional group formed on the PS surface for all gap distances, though the alcohol fraction decreases from 48% at 2 mm to 43% at 20 mm. The decrease in alcohol group can be attributed to a decrease in OH from about 2×10^{13} to about 8×10^{12} cm^{-3} from 1 to 20 mm. The decrease in total oxygen occupancy on the PS surface with increase in gap from 1 to 20 mm implies that O may be the most important gas-phase species for functionalizing the PS. However, for these conditions, the fluence of O atoms is in the saturation regime for all gaps.

B. Mole fraction of oxygen in inlet flow

The inlet mole fraction of oxygen in the He/O_2 mixture was varied from 0% to 10% to determine the consequences on the fractional occupancy of O on the PS surface after treatment. Water impurity was not included in the inlet for these cases to isolate the effects of changing the oxygen content on the end functionalization. O-occupancy using the base case power of 210 W is shown in Fig. 7(a) for the inlet mole fraction O_2 of 0% to 10 %. The densities of O and O_3 at the surface for this range of mole fractions of O_2 are shown in Fig. 7(b). The addition of even a small amount of O_2 (0.05%) is enough to produce significant O-occupancy (>50%) on the plasma-treated PS surface. As the inlet O_2 increases from 0.05% to 1%, there is a local maximum of 62.5% O-occupancy that occurs at 0.3% O_2 inlet fraction. When the inlet O_2 increases from 0.3% to 1%, the total O-occupancy decreases to 58% and continues to slowly decrease as the O_2 fraction increases to 3%. At O_2 inlet fractions higher than 3%, the total O-occupancy begins to fall off more steeply, from about 54% at 3% O_2 to 38% at 10% O_2.

These trends are largely attributable to the O-atom flux to the surfaces as a function of the O_2 inlet fraction. The increase in O-atom density simply results from the increase in the O_2 fraction. The rapid decrease in O-atom density at higher O_2 fraction results from the onset of O_3 formation with the higher O_2 mole fraction, increasing to an excess of 10^{17} cm^{-3} at a 10% inlet fraction. H abstraction from the PS backbone is the initiating event in PS functionalization. O atoms will abstract H from the backbone, whereas O_3 does not at any significant rate. So, the conversion of O to O_3 decreases the rate of initialization of PS functionalization.

The trends in total O-occupancy can be attributed to the dependence of the dominant oxidation products on O_2 fraction. From 0.3% to 1% O_2 fraction, the alcohol content is nearly

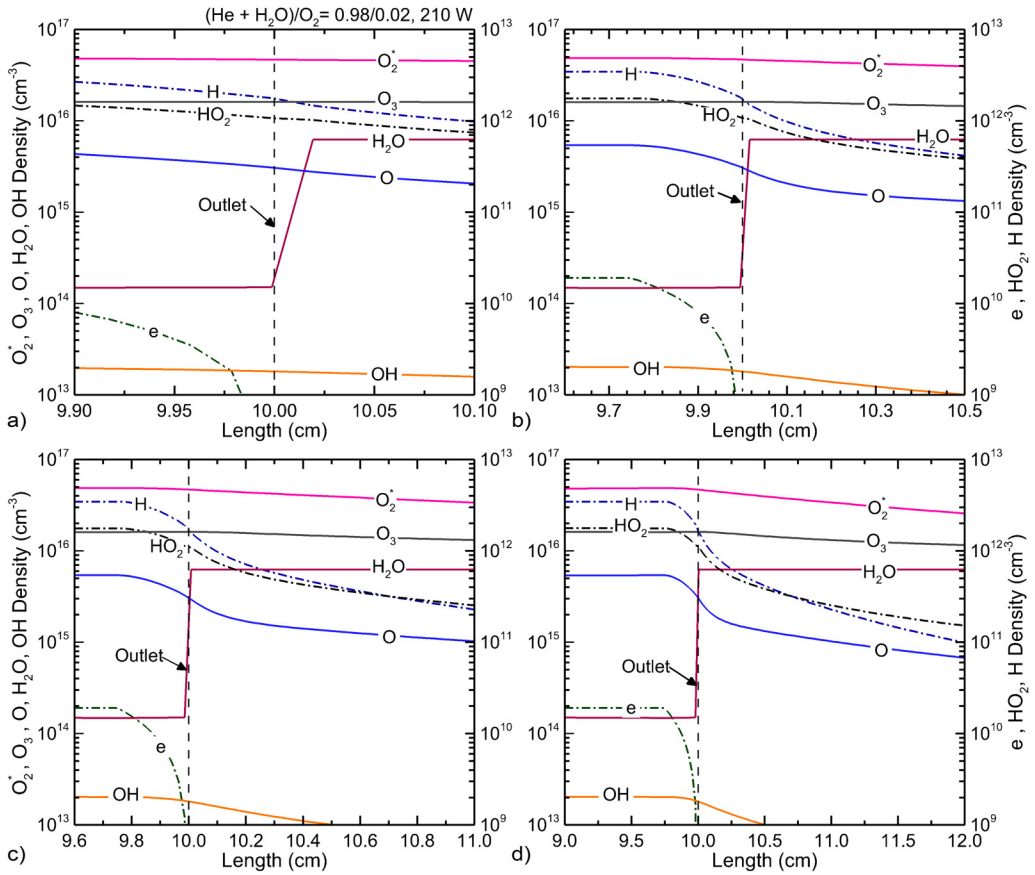

FIG. 5. Gas-phase species densities in the gap between the plasma head and the PS surface as a function of the gap distance. (a) 1, (b) 5, (c) 10, and (d) 20 mm. The densities of O_2^*, O_3, O, H_2O, and OH are shown on the left scale. The densities of e and HO_2 are shown on the right scale.

constant (49%–50%) while the cross-linked products decrease from 12% to 9%. With there being no OH production in the gas-phase, the ═C–OH alcohol bonding results dominantly from H abstraction by peroxy groups [Eq. (8)]. The increase in cross products results from an increase in the generation of peroxy groups with the larger flux of O_2, which then leads to cross-linking [Eq. (9)].

At low O_2 fractions, power is dissipated in the form of electron impact reactions to predominantly form O atoms by direct electron impact on O_2, by dissociative excitation transfer from excited states of He, and by dissociative recombination of O_2^+. With a small inlet fraction of O_2, the generation of O atoms is limited by the availability of O_2. In fact, the majority of O_2 can be dissociated. With the increase in O_2 inlet fraction, the O-atom density at the surface of the PS has a maximum value of 4.5×10^{15} cm^{-3} at an inlet O_2 fraction of about 0.4%, as shown in Fig. 7(b), which also corresponds to the local maximum in total O-occupancy on the PS surface. As the inlet mole fraction of O_2 increases, more pathways for nondissociative power dissipation become available in the form of vibrational, rotational, and nondissociative electronic excitation, which results in a decrease in the O flux to the substrate. The rapid decrease in O-atom density at higher O_2 fraction also results from the onset of O_3 formation with a higher O_2 mole fraction, increasing over 10^{17} cm^{-3} at 10% inlet fraction.

After a critical mole fraction of O_2 (0.8% for this case), O_3 becomes the dominant ROS. O initiates PS functionalization by abstracting H from the surface, but is unable to also passivate the newly formed alkyl site to form alkoxy. O_2 can passivate the alkyl site in the absence of adequate O to form peroxy sites, but these sites preferentially combine to form stabilizing cross-linked products. This reaction pathway would account for the smaller decrease in cross-linked products compared to the decrease in alcohol groups when O_3 dominates the ROS fluxes. Alkyl sites that have been passivated by O to form alkoxy sites propagate the initial functionalization step by abstracting H from neighboring sites to form the alcohol group, in effect resulting in the possibility for two H abstractions for every O-atom.

These trends suggest that the operating point that yields the highest degree of functionalization under these conditions is that which produces the highest O density (and flux) and the lowest O_3 density. If the O density has the largest effect on the final

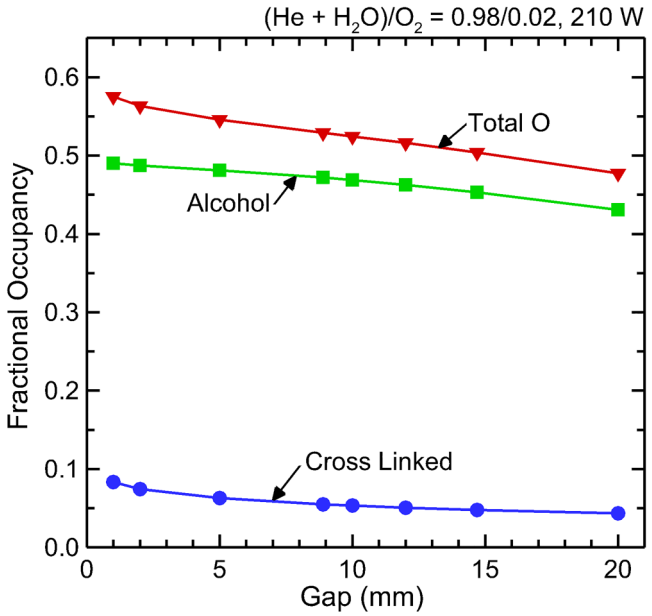

FIG. 6. Fractional occupancy of oxygen containing functional groups on the PS surface as a function of the gap distance of the plasma head from the surface for a power of 210 W. Plasma treatment time is 12 s, and post-treatment exposure to air is 200 s.

functionalization of the PS, it can also be concluded that H abstraction by ROS is the rate limiting step in the functionalization mechanism. Finite rates of H abstraction and passivation that differentiate between O and O_3 can always be overcome by increasing the ROS fluence to the point that the saturation regime is approached [Fig. 4(b)]. That is the case for powers >100–150 W for our conditions. The oxygen fraction (up to 5%) that yields the maximum O surface coverage is nearly independent of powers above 100–150 W as shown in Fig. 7(c). For lower powers (<100 W), the functionalization is not saturated and there is increasing sensitivity of O surface coverage to O_2 inlet fraction. As shown in Fig. 7(c), when not saturated (powers of 25 and 50 W), the decrease in O-atom flux and increase in O_3 flux with increasing O_2 inlet fraction produces a significant decrease in the O surface coverage.

C. Water vapor mole fraction

The most rapid H abstraction from the PS backbone to initiate functionalization occurs by the OH radical. There is some logic in having water vapor in the inlet flow to provide a flux of OH to the PS surface, while also producing other reactive oxygen species (ROS).[70,71] Water vapor in the inlet flow was varied as a fraction of the sum of $H_2O + O_2$, $r = [H_2O]/([H_2O] + [O_2])$. The water concentration r was varied from 0 to 100 for inlet gas compositions, $He/(H_2O + O_2) = 99.95/0.05$, 99.5/0.5, 99/1. The inlet fractions of $H_2O + O_2$ (0.05%–1%) were chosen based on our results and studies by others that suggest that the maximum densities of ROS

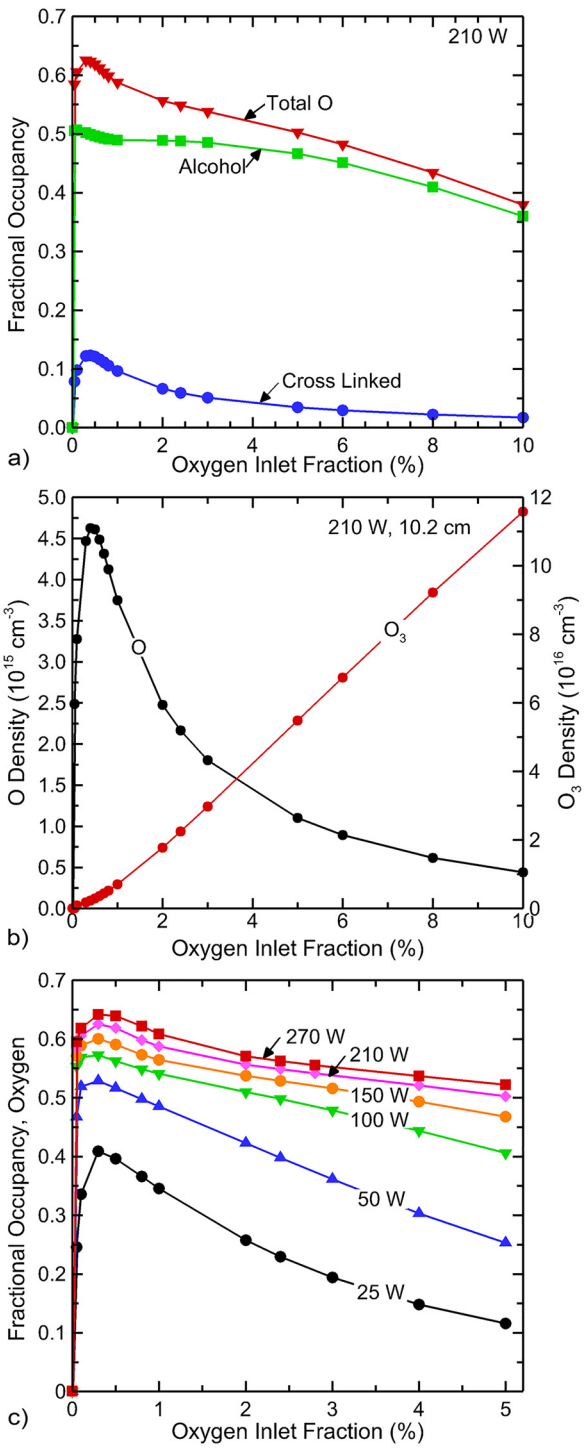

FIG. 7. Processing parameters as a function of O_2 fraction in the inlet flow (without H_2O impurity). (a) Fractional occupancy of oxygen containing functional groups on the PS surface for the RF power of 210 W. (b) Density of O atoms and O_3 for 210 W. (c) Total fractional occupancy of oxygen for different RF powers.

are produced when $H_2O + O_2$ composes 1% or less of the inlet flow.[71,72]

Plasma properties for $[H_2O] + [O_2]$=1.0% and $r = 0.09$, 0.9, and 0.99 are shown in Fig. 8. The delivery of ROS to the substrate is maximum at low inlet H_2O concentrations ($r < 0.1$) due to a higher rate of dissociation of O_2 and the presence of H from the dissociation of H_2O that acts as a reducing species. As the inlet H_2O concentration increases from $r = 0.09$ to 0.99, there is a decrease in O density at the surface from 1×10^{15} to 3×10^{13} cm^{-3} while the total OH density at the outlet changes little (6×10^{13} to 5.4×10^{13} cm^{-3}). OH and O can both be produced as dissociation products of H_2O, though OH formation occurs at a higher rate. When the inlet H_2O concentration increases beyond $r = 0.9$, OH is more abundant than O at the reactor outlet, though OH is depleted more quickly in the air gap so that a higher flux of O ultimately reaches the surface. O_3 also decreases (4×10^{15} to 9×10^{11} cm^{-3}) with increasing H_2O inlet fraction. A decrease in O_3 density corresponds with the decrease in O_2 fraction in the inlet, thereby reducing the likelihood of 3-body reactions.

The fractional occupancies of O-containing functional groups on the PS surface after treatment with plasmas having differing concentrations of water vapor for an inlet flow of $(H_2O + O_2) = 0.05\%$, 0.5%, and 1% are shown in Fig. 9. The general trend is decreasing O-occupancy with increasing inlet water vapor concentration. Increasing r (larger H_2O fraction) results in a decrease in total O-occupancy that also corresponds to a change in the dominant functional group from alcohol to cross-linked products. For low values of $(H_2O + O_2)$, the decrease in O-occupancy is nearly linear with the decrease in O_2 in the flow (increasing r). For larger values of $(H_2O + O_2)$, O-occupancy is fairly constant until $r = 0.5$, and nearly constant as a function of $(H_2O + O_2)$. Both of these trends indicate operation in a saturated regime. The one exception is the transition from no water in the flow ($r = 0$) to a finite amount ($r = 0.01$) where the O-occupancy decreases, for example, from 0.62 to 0.55. The introduction of OH into the flow to the substrate ultimately leads to lower O-occupancy.

The change in the dominant functional group at large r is due to the decrease in O-fluence with the decrease in O_2 fraction. The density of O at the substrate is 3.9–4.9 $\times 10^{14}$ cm^{-3} for $r = 0.1$ and 3.5–4.2 $\times 10^{13}$ cm^{-3} for $r = 0.9$. The density at the substrate of OH varies by less than a factor of 2 for all conditions (except for $r = 0$), clustered about 2×10^{13} cm^{-3}, as production of OH at low r is buoyed by the reactions of O(^{1}D) with H_2O. At a high r and large total mole fraction of $(H_2O + O_2)$, the flux of OH to the substrate is power limited, as the H_2O is not depleted in the gas phase. The major change in densities at the substrate is in the O_3 concentration, increasing from 9×10^{12} cm^{-3} [$r = 0.9$, $(H_2O + O_2) = 0.05\%$] to 4×10^{15} cm^{-3} [$r = 0.1$, $(H_2O + O_2) = 1\%$].

For conditions where the OH fluxes dominate over other ROS, OH initiates H abstraction from the PS with a higher probability than O and so O-occupancy should increase with increasing OH fluxes. However, the alkyl sites so produced are converted to peroxy sites by O_2 faster than they can be converted to alkoxy sites by the low O-fluence. Although there is an increase in alkoxy formation by increasing fluxes of O_3, the decrease in O-fluence dominates. These peroxy sites preferentially cross-link, effectively terminating the reaction. Cross-linking decreases the number of

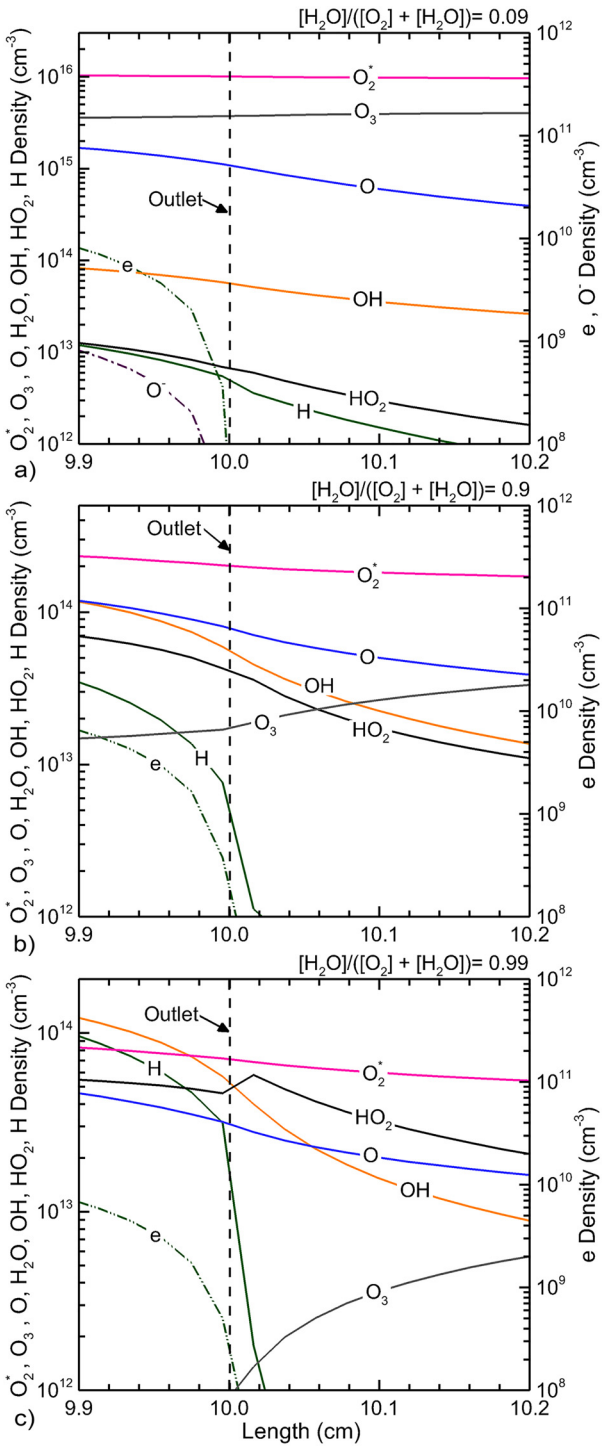

FIG. 8. Gas-phase species densities at the outlet and across the gap for He/O_2/H_2O plasma where the fraction of $[H_2O] + [O_2]$ is held constant at 1.0% for different ratios of inlet H_2O fraction, $r = [H_2O]/([O_2] + [H_2O])$. (a) $r = 0.09$, (b) 0.90, and (c) 0.99.

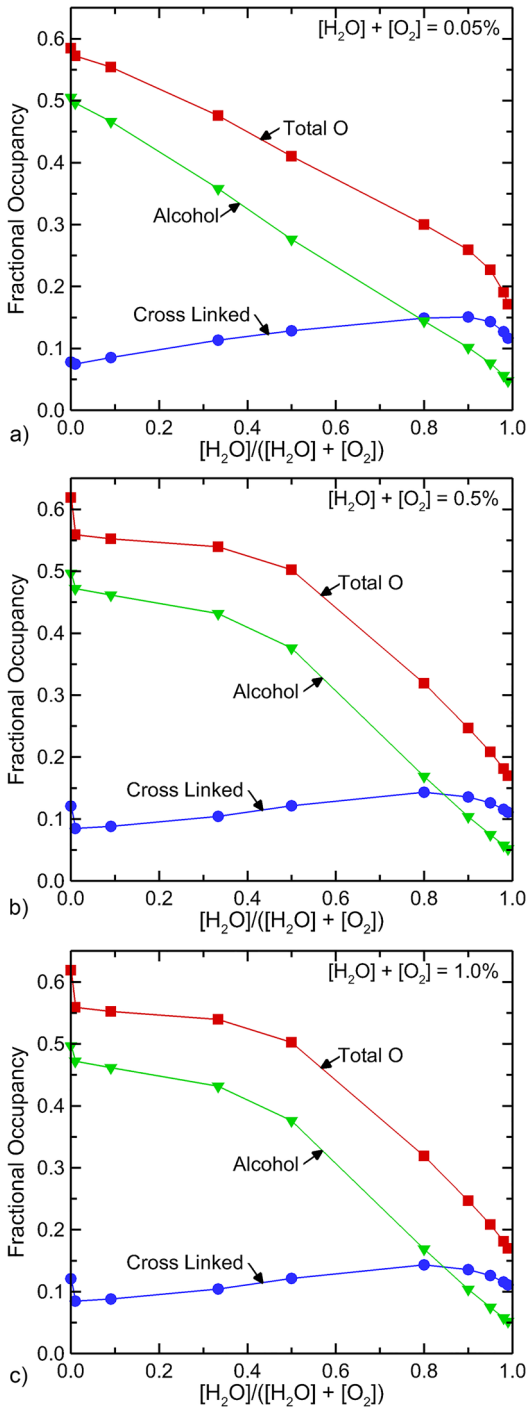

FIG. 9. Fractional occupancy of oxygen containing functional groups on the PS surface after the plasma treatment and exposure to air as a function of the ratio of H_2O to O_2 and total mole fraction of $H_2O + O_2$ in the inlet gas. Plasma treatment time = 12 s, Post-treatment time = 200 s. (a) $H_2O + O_2 = 0.5\%$, (b) $H_2O + O_2 = 0.8\%$, (c) $H_2O + O_2 = 1.0\%$.

surface sites available for functionalization (two sites are terminated for every cross-link) and leads to a lower total O-occupancy. Significant lowering of the O-fluence effectively eliminates a reaction pathway for alcohol formation (H abstraction of neighboring sites by alkoxy group). PS functionalization for these conditions is dominated by the O-atom fluence. Water vapor in the inlet shows promise for fine tuning the fractional coverage of the desired functional groups if the goal is not necessarily maximizing the O-coverage. Trends in O-coverage as a function of H_2O inlet concentration are the same regardless of the total gas composition for He-rich cases.

D. Relative humidity in ambient air

Water vapor in the inlet flow can have a significant effect on surface functionalization due to the resulting change in density and the mole fractions of OH, O, and O_3. Water vapor in the ambient air that diffuses into the plasma plume and in the post-treatment environment, has little effect on the functional groups on the PS surface. The fractional occupancy of functional groups on the PS surface was investigated as a function of the percent H_2O in the ambient air. The ambient H_2O was varied from 0% to 10%, while having no H_2O in the inlet flow to enable the assessment of water vapor in the ambient air on the end functionalization. There was little change in the surface oxygen coverage as a function of the H_2O fraction in the ambient for powers in the saturation regime. The most likely outcome of passivating free radical sites on the PS surface is the formation of peroxy by the far more abundant O_2. As such, the water vapor in the ambient has little influence on the final passivation products. Control of plasma-produced ROS has the greatest leverage for controlling the functionalization of the PS surface with plasma jets compared to controlling the ambient conditions.

VI. CONCLUDING REMARKS

A reaction mechanism for the surface functionalization of PS by a He/O_2 atmospheric pressure plasma jet was developed and implemented in a zero-dimensional, plug-flow global plasma chemistry model to predict fluxes of gas-phase species onto the PS surface. A surface site balance model was used to predict changes in the PS surface due to gas-phase and surface-surface reactions during plasma treatment and post-treatment exposure to the ambient. Fractional occupancy of oxygen on the PS surface was quantified as a function of plasma operating conditions. Results from this investigation suggest that alcohol functional groups and cross-linked products are the largest contributors to the oxygen-functionalization of the plasma-treated PS, consistent with experimental measurements for similar conditions. The high fraction of cross-linked products may explain the lack of long-term post-treatment changes in surface properties (as represented, for example, by a change in water contact angle) that occur with other plasma-treated polymers such as polypropylene. Control of the O-atom flux to the surface is the dominant factor in determining the degree of oxygen-functionalization with hydrogen abstraction from the PS backbone being the rate limiting step in the PS functionalization. Tuning of functionalization, that is, adjusting the proportion of different functional groups can be achieved by controlling the water vapor content in the inlet flow to

the plasma. Humidity in the ambient had little effect on this functionalization.

The O-atom coverage and functionality can be made less sensitive to operating conditions by using powers and O_2 inlet fractions that correspond to the saturation regime. Saturation in O-atom coverage and products occurs for O-atom fluences approaching 10^{17} cm^{-2}. With O-atom fluences below saturation, the O-coverage logically decreases, but more importantly, the system becomes more sensitive to changes in power, impurities, O_2 inlet fraction, post-plasma exposure, and the value of fluence itself. Obtaining reproducible results with a minimum of post-plasma change in properties will likely require operating at or near the saturation regime.

ACKNOWLEDGMENTS

This study was supported by Agilent Technologies. This material was also based on work supported by the U. S. Department of Energy, Office of Science, Office of Fusion Energy Sciences under Award No. DE-SC0020232 and the National Science Foundation (Nos. PHY-1902878 and IIP-1747739).

AUTHOR DECLARATIONS

Conflict of Interest

The authors have no conflicts of interest to disclose.

DATA AVAILABILITY

The data that support the findings of this study are available from the corresponding author upon reasonable request.

APPENDIX: ANALOGOUS GAS PHASE REACTIONS FOR ESTIMATING SURFACE REACTION PROBABILITIES

REFERENCES

[1]S. Guruvenket, G. M. Rao, M. Komath, and A. M. Raichur, Appl. Surf. Sci. **236**, 278 (2004).
[2]Y. Tamada and Y. Ikada, Polymer **34**, 2208 (1993).
[3]E. M. Liston, L. Martinu, and M. R. Wertheimer, J. Adhes. Sci. Technol. **7**, 1091 (1993).
[4]L. Carrino, G. Moroni, and W. Polini, J. Mater. Process. Technol. **121**, 373 (2002).
[5]J. Meichsner, M. Nitschke, R. Rochotzki, and M. Zeuner, Surf. Coat. Technol. **74–75**, 227 (1995).
[6]M. R. Sanchis, O. Calvo, O. Fenollar, D. Garcia, and R. Balart, J. Appl. Polym. Sci. **105**, 1077 (2007).
[7]H. R. Yousefi, M. Ghoranneviss, A. R. Tehrani, and S. Khamseh, Surf. Interface Anal. **35**, 1015 (2003).
[8]U. Schulz, P. Munzert, and N. Kaiser, Surf. Coat. Technol. **142–144**, 507 (2001).
[9]M. Lehocký, H. Drnovská, B. Lapčíková, A. M. Barros-Timmons, T. Trindade, M. Zembala, and L. Lapčík, Colloids Surf., A **222**, 125 (2003).
[10]I. Novák, V. Pollák, and I. Chodák, Plasma Processes Polym. **3**, 355 (2006).
[11]Y. Kusano, J. Adhes. **90**, 755 (2014).
[12]M. J. Shenton and G. C. Stevens, J. Phys. D: Appl. Phys. **34**, 2761 (2001).
[13]X. Lu, M. Laroussi, and V. Puech, Plasma Sou. Sci. Technol. **21**, 034005 (2012).
[14]A. Schütze, J. Y. Jeong, S. E. Babayan, J. Park, G. S. Selwyn, and R. F. Hicks, IEEE Trans. Plasma Sci. **26**, 1685 (1998).
[15]N. Gomathi, A. Sureshkumar, and S. Neogi, Curr. Sci. **94**, 1478 (2008).
[16]S. Yonson, S. Coulombe, V. Léveillé, and R. L. Leask, J. Phys. D: Appl. Phys. **39**, 3508 (2006).
[17]P. K. Chu, J. Y. Chen, L. P. Wang, and N. Huang, Mater. Sci. Eng. R Rep. **36**, 143 (2002).
[18]O. M. Ba, P. Marmey, K. Anselme, A. C. Duncan, and A. Ponche, Colloids Surf., B **145**, 1 (2016).
[19]P. Luan, V. S. Santosh, K. Kondeti, A. J. Knoll, P. J. Bruggeman, and G. S. Oehrlein, JVSTA **37**, 031305 (2019).
[20]A. Vesel, R. Zaplotnik, G. Primc, and M. Mozetič, Polymers **12**, 87 (2020).

TABLE III. Analogous gas-phase reactions for surface reaction mechanism.

	Reaction in Table II	Analogous reaction	Rate coefficient (cm^3 s^{-1})	Source
	Gas-phase surface reactions			
3	$O + R_b–H \rightarrow OH + R_b–•$	Benzene + OH → Phenyl + H_2O	6.61×10^{-15}	est (Ref. 47)
6	$OH + R_b–H \rightarrow H_2O + R_b–•$	Benzene + OH → Phenyl + H_2O	6.61×10^{-15}	Ref. 47
11	$O + R_b–• \rightarrow R_b–O•$	Estimated as gas kinetic.	1×10^{-10}	est (Ref. 29)
14	$O_2 + R_b–• \rightarrow R_b–OO•$	Phenyl + O_2 → $C_6H_5OO•$	5.83×10^{-12}	Ref. 48
17	$O_3 + R_b–• \rightarrow R_b–OO• + O_2$	Estimated as gas kinetic.	1×10^{-10}	est (Ref. 29)
18	$O + R_b–O• \rightarrow R_b–OO•$	$C_6H_5O + O• \rightarrow C_6H_5OO•$	6.26×10^{-13}	Ref. 49
21	$NO + R_b–O• \rightarrow R_b–• + NO_2$	C_6H_5O + NO → products	1.80×10^{-12}	Ref. 50
24	$OH + R_b–OH \rightarrow R_b–O• + H_2O$	Phenol + OH → $C_6H_5O + H_2O$	2.18×10^{-12}	Ref. 47
	Surface- surface reactions			
41	$R_b–• + R_2–OH \rightarrow R_b–H + R_2–O•$	C_2H_5OH + Phenyl → Benzene + CH_3CH_2O	1.0×10^{-14}	Ref. 51
42	$R_b–• + R_3–OH \rightarrow R_b–H + R_3–O•$	C_2H_5OH + Phenyl → Benzene + CH_3CH_2O	1.0×10^{-14}	Ref. 51
	Gas-phase termination reactions			
49	$H + R_b–• \rightarrow R_b–H$	Phenyl + H → Benzene	1.63×10^{-10}	Ref. 52
53	$OH + R_b–O• \rightarrow R_b–OOH$	$C_6H_5O + OH \rightarrow C_6H_5OOH$	9.29×10^{-22}	Ref. 53
54	$HO_2 + R_3–O• \rightarrow R_3–OH$	$CH_3O + HO_2 \rightarrow CH_3OH + O_2$	4.7×10^{-11}	Ref. 54
55	$HO_2 + R_2–O• \rightarrow R_2–OH$	$CH_3O + HO_2 \rightarrow CH_3OH + O_2$	4.7×10^{-11}	Ref. 54

[21]Y. Ren, C. Wang, and Y. Qiu, Surf. Coat. Technol. **202**, 2670 (2008).
[22]N. De Geyter, R. Morent, and C. Leys, Surf. Interface Anal. **40**, 608 (2008).
[23]L. Lianos, D. Parrat, T. Q. Hoc, and T. M. Duc, J. Vac. Sci. Technol., A **12**, 2491 (1994).
[24]T. H. Chen, F. Y. Chung, W. F. Jiang, and C. Huang, Vacuum **186**, 110069 (2021).
[25]R. W. Paynter and H. Benalia, J. Electron Spectrosc. Relat. Phenom. **136**, 209 (2004).
[26]E. H. Lock, D. Y. Petrovykh, P. Mack, T. Carney, R. G. White, S. G. Walton, and R. F. Fernsler, Langmuir **26**, 8857 (2010).
[27]K. Fricke, K. Duske, A. Quade, B. Nebe, K. Schroder, K. D. Weltmann, and T. Von Woedtke, IEEE Trans. Plasma Sci. **40**, 2970 (2012).
[28]C. Wang and X. He, Surf. Coat. Technol. **201**, 3377 (2006).
[29]A. N. Bhoj and M. J. Kushner, J. Phys. D: Appl. Phys. **40**, 6953 (2007).
[30]R. Dorai and M. J. Kushner, J. Phys. D: Appl. Phys. **36**, 666 (2003).
[31]A. N. Bhoj and M. J. Kushner, J. Phys. D: Appl. Phys. **39**, 1594 (2006).
[32]J. K. Stille, R. L. Sung, and J. V. Kooi, J. Org. Chem. **30**, 3116 (1965).
[33]H. Sekiguchi, M. Ando, and H. Kojima, J. Phys. D: Appl. Phys. **38**, 1722 (2005).
[34]J. F. Rabek and B. Ranby, J. Polym. Sci. Polym. Chem. Ed. **12**, 295 (1974).
[35]R. C. Longo, A. Ranjan, and P. L. G. Ventzek, ACS Appl. Nano Mater. **3**, 5189 (2020).
[36]A. M. Lietz and M. J. Kushner, J. Phys. D: Appl. Phys. **49**, 425204 (2016).
[37]R. Dorai, K. Hassouni, and M. J. Kushner, J. Appl. Phys. **88**, 6060 (2000).
[38]P. C. Schamberger, J. I. Abes, and J. A. Gardella, Colloids Surf., B **3**, 203 (1994).
[39]N. V. Bhat and D. J. Upadhyay, J. Appl. Polym. Sci. **86**, 925 (2002).
[40]Q. F. Wei, Mater. Charact. **52**, 231 (2004).
[41]A. Vesel, Surf. Coat. Technol. **205**, 490 (2010).
[42]T. Murakami, S. I. Kuroda, and Z. Osawa, J. Colloid Interface Sci. **200**, 192 (1998).
[43]J. J. Végh and D. B. Graves, Plasma Processes Polym. **6**, 320 (2009).
[44]See: "NIST Chemical Kinetics Database," https://kinetics.nist.gov/kinetics/
[45]J. Park, L. Wang, and M. C. Lin, Int. J. Chem. Kinet. **36**, 49 (2004).
[46]R. Atkinson, D. L. Baulch, R. A. Cox, J. Crowley, R. F. Hamspon, R. G. Hynes, M. E. Jenkin, M. J. Rossi, and J. Troe, Atmos. Chem. Phys. **6**, 3625 (2006).
[47]R. Knispel, R. Koch, M. Siese, and C. Zetzsch, Ber. Bunsen-Ges. Phys. Chem. **94**, 1375 (1990).
[48]T. Yu and M. C. Lin, J. Am. Chem. Soc. **116**, 9571 (1994).
[49]G. Da Silva and J. W. Bozzelli, J. Phys. Chem. A **112**, 3566 (2008).
[50]S. C. Xu and M. C. Lin, J. Phys. Chem. B **109**, 8367 (2005).
[51]J. Park, Z. F. Xu, K. Xu, and M. C. Lin, Proc. Combust. Inst. **34**, 473 (2013).
[52]L. B. Harding, Y. Georgievskii, and S. J. Klippenstein, J. Phys. Chem. A **109**, 4646 (2005).
[53]M. Batiha, A. H. Al-Muhtaseb, and M. Altarawneh, Int. J. Quantum Chem. **112**, 848 (2012).
[54]E. Assaf, C. Schoemaecker, L. Vereecken, and C. Fittshchen, Phys. Chem. Chem. Phys. **20**, 10660 (2018).
[55]P. Luan and G. S. Oehrlein, J. Phys. D: Appl. Phys. **51**, 135201 (2018).
[56]R. M. France and R. D. Short, Langmuir **14**, 4827 (1998).
[57]F. M. Petrat, D. Wolany, B. C. Schwede, L. Wiedmann, and A. Benninghoven, Surf. Interface Anal. **21**, 274 (1994).
[58]V. S. Santosh, K. Kondeti, Y. Zheng, P. Luan, G. S. Oehrlein, and P. J. Bruggeman, J. Vac. Sci. Technol., A **38**, 033012 (2020).
[59]P. Luan, A. J. Knoll, P. J. Bruggeman, and G. S. Oehrlein, J. Vac. Sci. Technol., A **35**, 05C315 (2017).
[60]P. Luan, V. S. S. K. Kondeti, A. J. Knoll, P. J. Bruggeman, and G. S. Oehrlein, J. Vac. Sci. Technol., A **37**, 031305 (2019).
[61]S. J. Moss, A. M. Jolly, and B. J. Tighe, Plasma Chem. Plasma Process. **6**, 401 (1986).
[62]R. M. France and R. D. Short, J. Chem. Soc., Faraday Trans. **93**, 3173 (1997).
[63]S. Vallon, B. Drévillon, and F. Poncin-Epaillard, Appl. Surf. Sci. **108**, 177 (1997).
[64]F. Poncin-Epaillard, J. C. Brosse, and B. Chevet, J. Adhes. Sci. Technol. **8**, 455 (1994).
[65]P. Bruggeman and R. Brandenburg, J. Phys. D: Appl. Phys. **46**, 464001 (2013).
[66]N. Balcon, G. Hagelaar, and J. P. Boeuf, IEEE Trans. Plasma Sci. **36**, 2782 (2008).
[67]S. Zhang, W. Van Gaens, B. Van Gessel, S. Hofmann, E. Van Veldhuizen, A. Bogaerts, and P. Bruggeman, J. Phys. D: Appl. Phys. **46**, 205202 (2013).
[68]A. Vesel, R. Zaplotnik, J. Kovac, and M. Mozetic, Plasma Sources Sci. Technol. **27**, 094005 (2018).
[69]A. Vesel, R. Zaplotnik, M. Mozetič, and G. Primc, Appl. Surf. Sci. **561**, 150058 (2021).
[70]D. X. Liu, F. Iza, X. H. Wang, M. G. Kong, and M. Z. Rong, Appl. Phys. Lett. **98**, 221501 (2011).
[71]D. X. Liu, P. Bruggeman, F. Iza, M. Z. Rong, and M. G. Kong, Plasma Sources Sci. Technol. **19**, 025018 (2010).
[72]D. X. Liu, M. Z. Rong, X. H. Wang, F. Iza, M. G. Kong, and P. Bruggeman, Plasma Processes Polym. **7**, 846 (2010).